



City Research Online

City, University of London Institutional Repository

Citation: Alsanat, H., Gunalan, S., Poologanathan, K., Guan, H. & Tsavdaridis, K. D. (2020). Numerical investigation of web crippling in fastened aluminium lipped channel sections under two-flange loading conditions. *Structures*, 23, pp. 351-365. doi: 10.1016/j.istruc.2019.10.012

This is the accepted version of the paper.

This version of the publication may differ from the final published version.

Permanent repository link: <https://openaccess.city.ac.uk/id/eprint/27022/>

Link to published version: <https://doi.org/10.1016/j.istruc.2019.10.012>

Copyright: City Research Online aims to make research outputs of City, University of London available to a wider audience. Copyright and Moral Rights remain with the author(s) and/or copyright holders. URLs from City Research Online may be freely distributed and linked to.

Reuse: Copies of full items can be used for personal research or study, educational, or not-for-profit purposes without prior permission or charge. Provided that the authors, title and full bibliographic details are credited, a hyperlink and/or URL is given for the original metadata page and the content is not changed in any way.

City Research Online:

<http://openaccess.city.ac.uk/>

publications@city.ac.uk



City Research Online

City, University of London Institutional Repository

Citation: Alsanat, H, Gunalan, S, Poologanathan, K, Guan, H and Tsavdaridis, KD ORCID: 0000-0001-8349-3979 (2020). Numerical investigation of web crippling in fastened aluminium lipped channel sections under two-flange loading conditions. Structures, 23, doi: 10.1016/j.istruc.2019.10.012

This is the draft version of the paper.

This version of the publication may differ from the final published version.

Permanent repository link: <https://openaccess.city.ac.uk/id/eprint/27022/>

Link to published version: <http://dx.doi.org/10.1016/j.istruc.2019.10.012>

Copyright: City Research Online aims to make research outputs of City, University of London available to a wider audience. Copyright and Moral Rights remain with the author(s) and/or copyright holders. URLs from City Research Online may be freely distributed and linked to.

Reuse: Copies of full items can be used for personal research or study, educational, or not-for-profit purposes without prior permission or charge. Provided that the authors, title and full bibliographic details are credited, a hyperlink and/or URL is given for the original metadata page and the content is not changed in any way.

City Research Online:

<http://openaccess.city.ac.uk/>

publications@city.ac.uk

1 **Numerical investigation of web crippling in fastened aluminium**
2 **lipped channel sections under two-flange loading conditions**

3
4 **Husam Alsanat**

5 School of Engineering and Built Environment, Griffith University
6 Gold Coast campus, QLD, 4222, Australia

7 School of Engineering, Al-Hussein Bin Talal University, Ma'an, Jordan

8 **Shanmuganathan Gunalan**

9 School of Engineering and Built Environment, Griffith University
10 Gold Coast campus, QLD, 4222, Australia

11 **Keerthan Poologanathan**

12 Faculty of Engineering and Environment, University of Northumbria,
13 Newcastle, UK

14 **Hong Guan**

15 School of Engineering and Built Environment, Griffith University
16 Gold Coast campus, QLD, 4222, Australia

17 **Konstantinos Daniel Tsavdaridis**

18 School of Civil Engineering, University of Leeds, LS2 9JT, Leeds, UK
19

20 **Abstract**

21 Aluminium alloys have recently been utilised in the fabrication of thin-walled members using
22 a roll-forming technique to produce purlins, floor joists and other structural bearers. Such
23 members are often subjected to transversely concentrated loads which may possibly cause a
24 critical web crippling failure. Aluminium specifications do not explicitly provide clear design
25 guidelines for roll-formed members subjected to web crippling actions. Therefore, this study
26 was conducted to investigate the mechanism of web crippling for roll-formed aluminium lipped
27 channel (ALC) sections with flanges attached to supports (fastened) under two-flange loading
28 conditions. Based on the experimental works presented in a companion paper, numerical
29 simulations were conducted including an extensive parametric study covering a wide range of
30 ALC geometrical dimensions, bearing lengths, and 5052 aluminium alloy grade with H32, H36
31 and H38 tempers. The acquired web crippling data were then used to investigate the influence
32 of the flange restraints on the web crippling mechanism of the ALC sections. Furthermore, a
33 detailed assessment of the consistency and reliability of the currently available design rules
34 used in practice was carried out. The predictions of the web crippling design guidelines given
35 in the Australian, American and European specifications were found to be unsafe and

36 unreliable, whereas a good agreement was obtained between the predictions of our recently
37 proposed design guidelines and acquired web crippling results. Further a suitable Direct
38 Strength Method (DSM)-based design approach was developed in this study with associated
39 equations to predict the elastic buckling and plastic loads of fastened ALC sections under two-
40 flange loading conditions.

41 **Keywords:** Web crippling; Aluminium lipped channel sections; Two-flange loading
42 conditions; Fastened; Numerical simulations; Design guidelines.

43 **1 Introduction**

44 Structural applications of aluminium alloys have recently increased in building construction
45 industry. The inherent characteristics of aluminium alloys including light-weight, corrosion
46 resistance, and ease of fabrication and shaping have attracted designers' attention in a wide
47 range of building applications especially those in harsh industrial and marine environments [1].
48 Thin-walled members fabricated by aluminium alloys have recently been employed in the
49 construction and building industries as purlins, floor joists and other structural bearers, and
50 therefore are potentially susceptible to various types of instabilities similar to thin-walled steel
51 members. Such structural members are highly prone to concentrated loads applied transversely,
52 which may lead to localised failure to the web called web crippling.

53 In real-life scenarios, aluminium structural members supported by column, bearers or rafters
54 and highly loaded by joists, purlins or live loading may induce web crippling failure. Depends
55 on the locations of the load and support, four failure scenarios can be potentially occurred
56 according to the AISI Standard test method [2]. If the loading and support are in the same line
57 of action, the member fails under two-flange loading conditions (end-two-flange (ETF) and
58 interior-two-flange (ITF)), otherwise one-flange loading conditions (end-one-flange (EOF) and
59 interior-one-flange (IOF)) are experienced. These loading conditions are further classified in
60 terms of the flange restraints, such as unfastened and fastened. It is worth to mention that the
61 majority of the available studies, both experimental and numerical ones, were conducted on
62 unfastened members [3-13] while limited studies [14-20] have been undertaken on fastened
63 sections even though the latter is often found in common real-life practice.

64 Several finite element analysis methods were utilised in the past to simulate thin-walled
65 members under web crippling action. For fastened channel sections, Macdonald et al. [16]
66 performed non-linear finite element analysis on unfastened/fastened cold formed steel lipped
67 channel sections using ANSYS software. Recently, Janarthanan et al. [18] thoroughly

68 investigated the use of quasi-static analysis based on the explicit integration scheme in
69 ABAQUS. Fastened unlippped cold-formed steel channel sections were simulated under one-
70 flange loading conditions. Unlike static general non-linear analysis and quasi-static analysis
71 with implicit integration, Janarthanan et al. [18] found that explicit dynamic method have the
72 ability to overcome certain convergence issues that former mentioned methods often encounter.

73 Investigating web crippling for aluminium members has also gained increasing attention in the
74 last decade. Extruded aluminium sections under the web crippling action were mainly
75 investigated [21-27] while limited studies were performed on roll-formed sections [28-30].
76 Zhou and Young [23] conducted web crippling experimental and numerical investigations on
77 extruded square and rectangular hollow sections under the ETF and ITF loading conditions.
78 The sections were fabricated using 6061-T6 and 6063-T5 heat-treated aluminium alloys.
79 Nonlinear static analysis were employed for the simulations and the developed finite element
80 models were verified against the experiments. Chen et al. [26] further investigated the web
81 crippling behaviour and capacity of extruded square hollow sections by carrying out experiments
82 and numerical analyses. The influence of different boundary conditions, bearing lengths, web
83 slenderness and loading conditions on the ultimate capacity and the section ductility were
84 examined. Improved design rules were also developed based on a parametric study to estimate
85 the web crippling capacity of the sections under four loading conditions. Recently, Zhou and
86 Young [22] reported web crippling experimental and numerical studies of unfastened extruded
87 aluminium alloy (6063-T5 and 6061-T6) unlippped and lipped channel sections. The finite
88 element models were developed and analysed using nonlinear static analysis, and then used for
89 an extensive parametric study.

90 Alsanat et al. [28, 29] experimentally and numerically studied the web crippling failure of
91 unfastened ALC sections under two-flange loading conditions (ETF and ITF). A detailed
92 assessment of the AS/NZS 1664.1 [31], AS/NZS 4600 [32] and Eurocode 3 [33] specifications
93 was performed and suitable modifications were made to improve their accuracy and reliability.
94 Alsanat et al. [30] also experimentally investigated the web crippling capacity of the ALC
95 sections with flanges attached to the supports under both the ETF and ITF loading conditions,
96 and a new prediction approach was developed to estimate the increase in the web crippling
97 capacity due to the flange being restrained. It should be noted that extruded and roll-formed
98 aluminium sections behave differently under buckling instabilities. This is due to the nature of
99 manufacturing process as extruded members are fabricated with sharp corners while roll-

100 formed sections are produced with rounded corners. Therefore, roll-formed sections under web
101 crippling actions are generally exposed to eccentric loading which will significantly influence
102 the behaviour and capacity of the members.

103 Owing to the empirical nature of the current methods for predicting the web crippling capacity,
104 and the lack of numerical studies on fastened aluminium sections, this study was conducted to
105 numerically investigate the web crippling phenomenon of fastened ALC sections under two-
106 flange loading conditions and further investigate the influence of a wider range of parameters
107 on the web crippling behaviour and capacity of fastened ALC sections. Accurate and reliable
108 numerical models, using quasi-static analysis with explicit integration scheme in
109 ABAQUS/CAE, were firstly developed and then validated against the experimental results [30]
110 in terms of ultimate web crippling strength, load-vertical displacement response and failure
111 mode. Based on the validation, an extensive parametric study comprising a various geometrical
112 dimensions, bearing lengths, and aluminium alloy grades was carried out. The acquired web
113 crippling database, in conjunction with that reported in Alsanat et al. [29] for unfastened ALC
114 sections, were subsequently used to further explore the effect of restrained flanges on the main
115 parameters associated with web crippling. Moreover, a detailed assessment for the currently
116 available design rules was performed, and a DSM-based approach was developed in this study
117 to determine the web crippling capacity of fastened ALC sections under two-flange loading
118 conditions.

119 **2 Brief overview of experimental study**

120 Two series of web crippling tests, including 38 test specimens of the ALC sections with
121 restrained flanges under the ETF and ITF loading conditions, were previously conducted by
122 Alsanat et al. [30]. Aluminium alloy grade 5052-H36 was used in the fabrication of the
123 specimens. Figures 1 (a) and (b) show the test set-up of fastened ALC sections under the ETF
124 and ITF loading conditions, respectively, and Figure 1 (c) shows the section profile of a typical
125 ALC section. Five different sectional sizes were considered and loaded by high strength
126 bearing plate (bearing length (N) ranged from 25mm to 150 mm). The specimens were cut to a
127 specific length (L) according to AISI S909 [2] ($L = 3h$ and $L = 5h$ for ETF and ITF loading
128 conditions, respectively). Tables 1 and 2 summarise the dimensional details and the ultimate
129 capacities of the fastened ALC sections under the ETF and ITF loading conditions,
130 respectively. The top and bottom flanges of the specimen were attached to the bearing plates
131 using M12 bolt per flange. Note that the label “ETF-20025-N100” indicates that the loading

132 condition is ETF, the section height (d) is 200 mm, the thickness of the web (t) is 2.5 mm, and
133 the length of the bearing plate (N) is 100 mm.

134 **3 Finite element study**

135 The finite element (FE) model of fastened ALC specimens under web crippling actions is
136 described in this section in detail. The general purpose finite element program, ABAQUS
137 Version 6.14 [34] was employed for this task due to its exceptional capabilities in simulating
138 various structural elements under diverse loading scenarios. Quasi-static analysis with explicit
139 integration was performed to simulate the slow movement of the loading plate during the
140 experimental tests. It has been proven that such analysis has the ability to overcome certain
141 contact and convergence difficulties that implicit (static) integrator often encounters [35]. Note
142 that initial geometrical imperfections were not considered in the modelling process, as the
143 applied load generated from the contact between the load bearing plate and corner radius has a
144 large eccentricity with respect to the web portion. Natário, et al. [35] and Sundararajah et al.
145 [6] verified this by investigating the influence of several possible geometrical imperfections
146 for cold-formed steel lipped channel sections and found that their influence on the web
147 crippling capacity is less than 1%.

148 **3.1 Finite element type and mesh control**

149 The ALC sections were modelled using the general purpose S4R shell element, which is a
150 linear 4 node deformable element with reduced integration, allowing for finite strains and
151 changes in thickness. It has been proven that such type of element is suitable to simulate 3D
152 thin-walled members under web crippling actions [6, 35]. The loading and support bearing
153 plates were modelled using R3D4 discrete rigid elements since they are much stiffer compared
154 to the section itself.

155 To achieve a high accuracy of the finite element solution and minimise the computational time
156 of the analysis, the mesh size for numerical model were carefully selected. The details for mesh
157 size sensitivity analysis were reported by Alsanat et al. [29] for unfastened aluminium lipped
158 channel sections. Similar mesh size control is employed in this study. The lipped channel
159 section was modelled using mesh size of 5×5 mm, except the corners as the finer mesh of 5×1
160 mm was assigned to ensure appropriate transformation of the internal stress throughout the
161 web-flange junction.

162 3.2 Material properties

163 The material properties employed in the numerical analysis were gained from conducting
164 tensile coupon tests [30]. Fifteen coupons were extracted from the flat portion of the web of
165 the sections and tested. Table 3 gives the mechanical properties including elastic modulus (E),
166 static 0.2% tensile proof stress ($\sigma_{0.2}$) and ultimate tensile strength (σ_u) and strain (ϵ_u). The
167 engineering stress-strain curves obtained from coupon tests were converted to the true stress–
168 strain curves using Equations (1) and (2), since web crippling problems may involve high
169 plastic strains.

$$170 \quad \sigma_{true} = \sigma_{eng}(1 + \epsilon_{eng}) \quad (1)$$

$$171 \quad \epsilon_{true} = \ln(1 + \epsilon_{eng}) \quad (2)$$

172 where σ_{true} is the true stress (MPa), ϵ_{true} is the true strain, σ_{eng} is the engineering stress (MPa)
173 and ϵ_{eng} is the engineering strain.

174 Figure 2 shows the typical engineering and true stress-strain curves for the 5052 H36
175 aluminium alloy. The material model consists of two parts; the elastic modulus of the material
176 was identified to represent the elastic region while the plastic region was considered using the
177 true plastic stress-strain curve. Despite the fact that the material properties for the corners differ
178 from the web portion, the acquired material properties were used to model the whole section
179 including the corners. It is believed that the changes in the material properties for the corners
180 will not affect the ultimate web crippling capacity and behaviour for models failed in pure web
181 crippling. Also, the models experienced flange crushing were not considered in proposing
182 design rules.

183 3.3 Contact and constraint definition

184 The interactions between the bearing plate, the ALC sections and the bolts were modelled
185 precisely using Contact Pair and Multi-Point Constraint (MPC) algorithms in ABAQUS [34].
186 The Contact Pair algorithm with a Penalty contact method was employed to simulate contact
187 between deformable bodies (lipped channel section) and rigid elements (bearing plates). The
188 contact formulation was assumed to be “Hard”, and a friction coefficient of 0.4 was assigned
189 to avoid any frictional slip. To simulate the bolt connection, Multi-Point Constraint (MPC)
190 with rigid ties were identified between the rigid plate and the bolt hole perimeter (Figure 3).
191 Such constraint can prevent any rotational movement of the flange during the analyses so that
192 the fastened condition can be adequately represented.

193 3.4 Boundary conditions and loading

194 The boundary conditions were precisely assigned to the models to simulate the actual
195 experimental scenario. Reference Points were used to assign the boundary conditions for the
196 loading and support plates. Identical boundary conditions were assigned to both ETF and ITF
197 models. As shown in Figure 3, the U_x , U_y and U_z translational movements, and R_y and R_z
198 rotations were fully restrained at the support plate. The loading plate was restricted from U_x
199 and U_z translational movement and R_y and R_z rotations, however the vertical downward
200 movement (U_y) was permitted.

201 In the analysis, both Smooth Step and Mass Scaling options were implemented to reduce any
202 converge issues and accelerate the calculations. The Smooth Step Amplitude allowed the model
203 to deform smoothly in the initial stage of the analysis by reducing the displacement while Mass
204 Scaling options increased the mass density of the modelled elements which led to a significant
205 reduction of the number of time increment generated from the quasi-static analysis [34].

206 Simulating the actual experimental loading rate (2 mm/min) using Quasi-static analysis with
207 explicit integration is, in fact, highly time-consuming process (Natário et al. [34]). Therefore,
208 both artificial loading rates and Mass Scaling methods are often implemented to accelerate the
209 calculations. However, these methods may lead to a significant increase in the influence of the
210 inertial effects and noise on the results. Therefore, the loading rate and mass scaling values
211 were carefully assigned, and the kinetic-to-internal energy ratios were closely monitored. In
212 this study, the loading rate of 25mm/s (total applied displacement = 25 mm and total step time
213 = 1 s) with smooth step amplitude (ramp procedure), and a constant Mass Scaling factor of 100
214 was assigned in the analysis. Default values of linear bulk viscosity parameters (damping
215 coefficient value of 0.06) and quadratic bulk viscosity parameter (1.2) were assigned. Apart
216 from the very first instants of the simulations, the kinetic-to-internal energy ratios remained
217 below 5% during the analysis.

218 3.5 FEA Validation

219 The developed 38 numerical models were compared with the experiments in terms of the
220 ultimate capacity, load-vertical deformation responses and failure modes. The numerical web
221 crippling results (P_{FEA}) agreed very well with the experimental capacities ($P_{Exp.}$) for both the
222 ETF and ITF loading conditions as shown in Tables 1 and 2, respectively. The mean and COV
223 values of the $P_{Exp.}/P_{FEA}$ ratios are 0.96 and 0.05 for the ETF loading condition, respectively,
224 whereas these values are 0.99 and 0.05, respectively, for the ITF loading condition.

225 The load-vertical displacement responses and the failure modes obtained from the numerical
226 simulations were also validated with the experiments. The load-vertical displacement
227 responses of the numerical models were predicted including the post-failure stage, as presented
228 in Figures 4 (a) and (b) for the loading conditions of ETF and ITF, respectively. Even though
229 both comparisons show a strong agreement in the post-failure stages, the elastic stiffness
230 observed in the initial stage noticeably differ for both loading conditions. It is believed that the
231 measured vertical displacement was inevitably affected by the test rig settlement during the
232 tests. Such a difference was also observed by Sundararajan et al. [6]. The failure modes of ETF-
233 25025-N100 and ITF-10030-N100 specimens as observed in the experiments and numerical
234 analysis are compared in Figures 5 (a) and (b). In General, the numerical models are able to
235 simulate the experimental tests of fastened ALC sections under two-flange loading conditions.

236 It was observed from the experimental and numerical investigations that specimens under ITF
237 loading condition with 25 mm bearing plates experienced flange crushing failure. The
238 numerical load-vertical displacement responses were validated with the experimental
239 responses as shown in Figures 4 (c) for the ITF-20030-N25 specimen. Both the experimental
240 and the numerical responses exhibited the flange crushing behaviour. Figure 5 (c) shows the
241 agreement between the experimental and numerical failure modes of the ITF-25025-N25
242 specimen.

243 3.6 Parametric study

244 Based on the validated numerical models discussed in the previous section, a parametric study
245 was conducted to explore the influence of various parameters on the web crippling capacity of
246 fastened ALC sections under two-flange loading conditions. The acquired results obtained
247 from both experiments and parametric analyses will then be used to assess the suitability of the
248 design rules given in the current standards and Alsanat et al. [30]. New predictive Direct
249 Strength Method (DSM) approach will also be developed based on these results.

250 The parametric study details are summarised in Table 4 as follow: $50 \text{ mm} \leq N \leq 150 \text{ mm}$, 28
251 $\leq h/t \leq 130$ and $2 \text{ mm} \leq r_i \leq 8 \text{ mm}$. Additionally, aluminium alloy grade 5052 with hardening
252 of H32, H36 and H38 [31] were also considered. The length of specimens used in the
253 parametric study was $3d$ and $6d$ for the ETF and ITF loading conditions as recommended by
254 Alsanat et al. [29].

255 To consider the strain hardening effect, the bi-linear model proposed by Su et al. [36] for
256 aluminium material was implemented in the parametric analyses as shown in Figure 2. The

257 strain hardening slope (E_{sh}) and the ultimate strain (ε_u) can be calculate using Equations (3)
 258 and (4), respectively.

$$259 \quad E_{sh} = \frac{f_u - f_y}{C_2 \varepsilon_u - \varepsilon_y} \quad (3)$$

$$260 \quad \varepsilon_u = C_3 \left(1 - \frac{f_y}{f_u}\right) + C_4 \quad (4)$$

261 where $C_2 = 0.5$, $C_3 = 0.13$, and $C_4 = 0.059$ are constants for aluminium material, f_y is the yield
 262 stress, f_u is the material ultimate stress (MPa) and ε_y is the yield strain.

263 **4 The effect of fastened flanges**

264 The acquired parametric results for fastened ALC sections and the parametric data reported by
 265 Alsanat et al.'s [29] for unfastened sections were analysed to explore the influence of fastened
 266 flanges on the section ultimate web crippling capacity. Typically, fastening the flanges has a
 267 substantial effect on the capacity of the ALC sections. Such restraint prevents flange rotation
 268 and consequently results in a significant reduction in the out-of-plane moment imposed on the
 269 web from the eccentric load. Hence, the overall capacity of the section will substantially
 270 increase. This can be confirmed by Figures 6 (a) and (b) which display the difference between
 271 unfastened and fastened specimens, respectively, in terms of failure modes.

272 Figure 7 compares the web crippling capacities of unfastened and fastened sections under the
 273 ETF and ITF loading conditions. Generally, flange restraining has more influence on the ETF
 274 sections, up to 88% increased strength with an average of 59%, whereas , the ITF sections can
 275 gain up to 45% more capacity with an average of 22%.

276 Figures 8 and 9 illustrate the influences of the major geometrical parameters N/t and h/t ,
 277 respectively on the web crippling capacity ratios (P_F/P_U) of the ALC sections. Figure 8 shows
 278 the P_F/P_U ratio versus the bearing length ratio (N/t) for three different inside bent radii (r_i)
 279 under both the ETF and ITF loading conditions. It can be seen that increasing the bearing length
 280 ratio (N/t) results in a considerable increase to the capacity ratio (P_F/P_U) of ALC sections. The
 281 P_F/P_U ratios for the ETF specimens are more sensitive to such influence than the ITF
 282 specimens. It is also shown that varying the inside bend radii (r_i) for the same N/t has a minimal
 283 influence on the P_F/P_U ratio. Figure 9 demonstrates the effects of the web slenderness ratios
 284 (h/t) on P_F/P_U ratios for three bearing lengths (N) under the ETF and ITF loading conditions.
 285 As h/t ratio increases, a relatively small increase in the P_F/P_U ratios was observed compared to
 286 the influence of N/t ratios. The ETF specimens loaded with the small bearing plates ($N = 50\text{mm}$)

287 are more sensitive to the change in the h/t ratio compared to the large bearing plates ($N =$
288 100mm and 150mm), whereas the ITF specimens behave similarly regardless of the change in
289 the bearing length.

290 The relationship between the web crippling capacity ratio (P_F/P_U) of the ALC sections and the
291 geometrical factor Nh/t^2 was investigated based on the experimental data reported by Alsanat
292 et al [28, 30] covering both unfastened and fastened specimens. Increasing the Nh/t^2 factor leads
293 to a nonlinear increase the P_F/P_U and novel predictive approach (fastening factor (k_f)) was
294 proposed in Alsanat et al [30] to estimate the increased capacity ratio (P_F/P_U) of fastened ALC
295 section (Equation (5)).

$$296 \quad k_f = 0.6 \left(\frac{Nh}{t^2} \right)^a \geq 1 \quad (5)$$

297 where the coefficient $a = 0.126$ and 0.095 for the ETF and ITF loading conditions, respectively.

298 Figures 10(a) and (b) present all the experimental and numerical web crippling capacity ratios
299 (P_F/P_U) against the geometrical factor Nh/t^2 for the ETF and ITF loading conditions,
300 respectively. The mean values of the P_F/P_U to the predicted (k_f) ratios are 1.00 and 0.97 for the
301 ETF and ITF loading conditions, respectively, while the corresponding COV values is 0.06
302 both loading conditions. This indicates the suitability of the new fastening factor approach to
303 predict the increased web crippling capacity of wide-ranged fastened ALC sections under two-
304 flange loading conditions.

393 **5 Current design rules**

394 5.1 International specifications

395 A detailed assessment to the accuracy of design guidelines recommended in the AS/NZS
396 1664.1 [31], AS/NZS 4600 [32] and Eurocode 3 [33] were conducted by comparing them with
397 experimental and numerical parametric results. It should be mentioned that the predictions of
398 the web crippling capacities using these specifications, apart of AS/NZS 4600 [32], are not
399 differentiated between the sections with fastened and unfastened support conditions. Moreover,
400 the design provisions given in Eurocode 9 [37] for aluminium sheeting structures were
401 excluded herein due to their limitation to sections with multi-webs. The three specifications
402 mentioned above are briefly introduced below outlining their respective prediction equations.

403 5.1.1 AS/NZS 1664.1 [31] for aluminium structures

$$404 \quad P_{AS1664} = \frac{1.2t^2 \sin \theta (0.46f_y + 0.02\sqrt{Ef_y})(N + C_{w2})}{C_{w3} + r_i(1 - \cos \theta)} \quad (\text{ETF}) \quad (6)$$

$$405 \quad P_{AS1664} = \frac{t^2 \sin \theta (0.46f_y + 0.02\sqrt{Ef_y})(N + C_{w1})}{C_{w3} + r_i(1 - \cos \theta)} \quad (\text{ITF}) \quad (7)$$

406 where $C_{w1} = 140\text{mm}$, $C_{w2} = 33\text{mm}$, $C_{w3} = 10\text{mm}$, t is the web thickness, N is the bearing
 407 length (mm), r_i is the internal bent radius (mm); E is the elastic modulus (MPa), f_y is the 0.2%
 408 static yield stress (MPa), and θ is the angle between the web surface and the bearing surface
 409 plane ($\theta = 90^\circ$).

410 5.1.2 AS/NZS 4600 [32] for cold-formed steel structures

$$411 \quad P_{AS4600} = Ct^2 f_y \sin \theta \left(1 - C_R \sqrt{\frac{r_i}{t}}\right) \left(1 + C_N \sqrt{\frac{N}{t}}\right) \left(1 - C_h \sqrt{\frac{h}{t}}\right) \quad (8)$$

412 where h is the flat portion of the web (mm); C , C_R , C_N , C_h are the geometrical coefficients given
 413 in Table 5. Note that in Equation (6), the following conditions $h/t \leq 200$, $N/t \leq 210$, $r_i/t \leq$
 414 12 , $N/h \leq 2$, and $\theta = 90^\circ$ must be satisfied.

415 5.1.3 Eurocodes 3 [33] for cold-formed steel structures

$$416 \quad P_{EC3} = \frac{k_1 k_2 k_3 f_y t^2}{\gamma_{M1}} \left[6.66 - \frac{d_w}{64t}\right] \left[1 + 0.01 \frac{N}{t}\right] \quad (\text{ETF}) \quad (9)$$

$$417 \quad P_{EC3} = \frac{k_3 k_4 k_5 f_y t^2}{\gamma_{M1}} \left[21 - \frac{d_w}{16.3t}\right] \left[1 + 0.0013 \frac{N}{t}\right] \quad (\text{ITF}) \quad (10)$$

418 where:

$$419 \quad k_1 = 1.33 - \frac{f_y}{690.9};$$

$$420 \quad k_2 = 1.15 - 0.15 \frac{r_i}{t} \quad (0.5 \leq k_5 \leq 1.0);$$

$$421 \quad k_3 = 0.7 + 0.3 \left(\frac{\theta}{90}\right)^2;$$

$$422 \quad k_4 = 1.22 - \frac{f_y}{1036.4};$$

423 $k_5 = 1.06 - 0.06 \frac{r_i}{t} \quad (k_5 \leq 1.0);$

424 d_w is the web height between the flange mid-lines in mm; γ_{M1} is the partial safety factor
 425 ($\gamma_{M1} = 1$) and θ is equal to 90° .

426 The mean and COV values of the web crippling capacities ratios ($P_{Exp.-FEA}/P_{predicted}$) for the
 427 ETF and ITF loading conditions are summarised in Table 5. Generally, the design rules
 428 provided by the aforementioned specifications, apart from AS/NZS 1664.1 [31] for the ITF
 429 loading condition, overestimate the web crippling capacity of fastened ALC sections. The mean
 430 values of $P_{Exp.-FEA}/P_{predicted}$ ratios are ranging from 0.55 to 0.87 with the COV values between
 431 0.11 and 0.26 for both the ETF and ITF loading conditions. The AS/NZS 1664.1 [31]
 432 predictions agree reasonably well for the ITF loading condition with the mean and COV values
 433 equalling 1.04 and 0.13, respectively. Figures 11 (a) and (b) show the comparisons between
 434 the predicted capacities ($P_{predicted}$) obtained from the current design guidelines and the ultimate
 435 web crippling capacity capacities ($P_{Exp.-FEA}$) under the ETF and ITF loading conditions,
 436 respectively.

437 5.2 Modified design rules

438 Alsanat et al. [28] improved the accuracy of the design rules obtained from the AS/NZS 1664.1
 439 [31], AS/NZS 4600 [32] and Eurocode 3 [33] specifications for unfastened ALC sections by
 440 modifying them based on experimental tests, in which the test specimens had their h/t ranging
 441 from 30 to 100, $r_i = 5$ mm and the aluminium alloy grade being 5052 H36. In this study,
 442 comparisons between the predictions of the modified Equations (11)–(15) (where k_f is the
 443 fastening factor according to Equation (5) and the wide-ranged parametric and experimental
 444 data for fastened ALC sections were carried out.

445 5.2.1 Modified AS/NZS 1664.1

446
$$P_{AS1664(Modi.)} = k_f \frac{C_1 t^2 \sin \theta (0.46 f_y + 0.02 \sqrt{E f_y}) (N + C_{w2})}{C_{w3} + r_i (1 - \cos \theta)} \left(1 - C_{h1} \sqrt{\frac{h}{t}} \right) \quad (\text{ETF}) \quad (11)$$

447
$$P_{AS1664(Modi.)} = k_f \frac{C_2 t^2 \sin \theta (0.46 f_y + 0.02 \sqrt{E f_y}) (N + C_{w1})}{C_{w3} + r_i (1 - \cos \theta)} \left(1 - C_{h2} \sqrt{\frac{h}{t}} \right) \quad (\text{ITF}) \quad (12)$$

448 where $C_1 = 0.31$, $C_2 = 258$, $C_{w1} = 780\text{mm}$, $C_{w2} = 238\text{mm}$, $C_{w3} = 10\text{mm}$, $C_{h1} = 0.05$ and $C_{h2} =$
 449 0.025 .

450 5.2.2 Modified AS/NZS 4600

$$451 \quad P_{As4600(modi.)} = k_f C t^2 \sqrt{E f_y} \sin \theta \left(1 - C_R \sqrt{\frac{r_i}{t}} \right) \left(1 + C_N \sqrt{\frac{N}{t}} \right) \left(1 - C_h \sqrt{\frac{h}{t}} \right) \quad (13)$$

452 where the values of the proposed geometrical coefficients are summarised in Table 5.

453 5.2.3 Modified EC3

$$454 \quad P_{EC3(Modi.)} = k_f \frac{0.028 k_1 k_2 k_3 \sqrt{E f_y} t^2}{\gamma_{M1}} \left[6.66 - \frac{d_w}{64t} \right] \left[1 + 0.01 \frac{N}{t} \right] \quad (\text{ETF}) \quad (14)$$

455

$$456 \quad P_{EC3(Modi.)} = k_f \frac{0.034 k_3 k_4 k_5 \sqrt{E f_y} t^2}{\gamma_{M1}} \left[21 - \frac{d_w}{16.3t} \right] \left[1 + 0.0013 \frac{N}{t} \right] \quad (\text{ITF}) \quad (15)$$

457 The mean and COV values of the web crippling capacity ratios ($P_{Exp.-FEA}/P_{predicted}$) using the
 458 modified Equations (11)-(15) are summarised in Table 6 for the ETF and ITF loading
 459 conditions. The comparison shows that the modified equations are able to accurately predict
 460 the web crippling capacity for both loading conditions with reasonable mean and COV values
 461 ranging from 0.99 to 1.10 and 0.05 to 0.10, respectively. It can be concluded that the web
 462 crippling capacity formulae incorporating the fastening factor can accurately predict the
 463 increased capacities of the ALC sections under two-flange loading conditions when the flanges
 464 are restrained to the supports as shown in Figures 12 (a) and (b).

465 6 Direct strength method

466 Schafer [38] developed the Direct Strength Method (DSM) approach to determine the ultimate
 467 capacity of thin-walled members. This method has been successfully employed to estimate the
 468 capacity of cold-formed steel member under compression, bending and shear actions based on
 469 their elastic and yield capacities. However, further improvement to this method is still needed
 470 for the web crippling design of thin-walled aluminium members. In this study, the DSM-based
 471 design equations are proposed for predicting the web crippling capacities (P_n) of fastened ALC
 472 sections under two-flange loading conditions, based on the results from experiments [30] and

473 those obtained from the present numerical parametric analyses. For this purpose, critical
 474 buckling and yield loads of fastened ALC sections are determined by the FE elastic buckling
 475 analysis and the Yield-Line Theory (YLT), respectively.

476 6.1 Elastic buckling load

477 The elastic buckling load for conventional plates is generally determined using Equation (16).
 478 However, such approach is rather inaccurate in predicting the elastic capacity of lipped channel
 479 sections due to the complex interaction between the web, flanges and corners elements and
 480 therefore numerical elastic buckling analysis is often implemented instead. In this study,
 481 ABAQUS was employed to conduct elastic buckling analyses to estimate the critical buckling
 482 loads of fastened ALC sections under ETF and ITF loading conditions.

$$483 \quad P_{cr} = \frac{\pi^2 E k_{cr} t^3}{12(1-\nu^2)d} \quad (16)$$

484 where k_{cr} is the buckling coefficient and ν is the the Poisson ratio (0.33 for aluminium).

485 Figure 13 shows the established numerical models with the associated boundary conditions to
 486 predict the critical buckling load of fastened ALC sections under the ETF and ITF loading
 487 conditions. The bottom flange at the supports was prevented from translational movement in
 488 all directions (displacements U_x , U_y , and U_z) for both loading conditions. For the loaded area
 489 on the top flange, Reference Point (RP) was implemented with MPC rigid tie connections to
 490 assign the boundary conditions (U_x , U_z , R_y , and R_z were fixed), and a unit load was assigned to
 491 the vertical direction (U_y). The Subspace Eigen Extraction method was used in the linear
 492 analysis, and the first Eigen mode (minimum buckling capacity) was selected. A total of thirty-
 493 eight numerical models were simulated for the ETF and ITF loading conditions and their elastic
 494 buckling capacities $P_{cr(FEM)}$ are summarised in Tables 7 and 8, respectively.

495 The elastic critical buckling loads obtained from the numerical analyses were used to calculate
 496 the elastic buckling coefficient ($k_{cr(FEA)}$) using Equation (16), and the results are summarised in
 497 Tables 7 and 8, for the ETF and ITF loading conditions, respectively. The coefficient k_{cr} is
 498 typically influenced by both sectional geometry and the bearing length, and hence can be
 499 expressed using empirical expressions. A linear relationship was found between $k_{cr(FEA)}$ and the
 500 bearing length to section height ratio (N/d), as shown in Figure 14. Thus, a simplified approach
 501 (Equation (17)) was developed in this study to determine the elastic buckling coefficients
 502 ($k_{cr(Prop.)}$) of the fastened ALC sections under both loading conditions.

$$503 \quad k_{cr(Prop.)} = C_{b,1} + C_{b,2} \frac{N}{d} \quad (17)$$

504 where $C_{b,1}=1$ and $C_{b,2}=3$ for the ETF loading condition, and $C_{b,2}=3.4$ and $C_{b,2}=2$ for the
 505 ITF loading condition.

506 The FE buckling loads ($P_{cr(FEM)}$) and the proposed buckling loads ($P_{cr(Prop.)}$), calculated by
 507 substituting Equation (15) into Equation (16), are compared in Tables 7 and 8 for the ETF and
 508 ITF loading conditions, respectively. The mean value of $P_{cr(FEM)}/P_{cr(Prop.)}$ is 1.00 for both
 509 loading conditions, whereas the corresponding COV values are 0.03 and 0.02. This indicates
 510 that the proposed elastic buckling load ($P_{cr(Prop.)}$) incorporating the fastening factor agrees well
 511 with the corresponding numerical buckling load ($P_{cr(FEM)}$) for fastened ALC sections under both
 512 ETF and ITF loading conditions.

513 6.2 Yield load

514 Determining the yield load (P_y) is the other key aspect of the DSM-based design method in
 515 addition to the buckling load (P_{cr}). Generally, simplified approaches can be used for beams,
 516 columns, beam-columns under global, distortional and local buckling modes. However, for
 517 members under web crippling actions, highly localised deformations and the associated non-
 518 uniform stresses further obscure the definition of the yield load. Natário et al. [39, 40]
 519 thoroughly investigated the plastic mechanism of different cold-formed steel sections including
 520 built-up I-section, Z- section (fastened/unfastened), C-section (unlipped/lipped and
 521 fastened/unfastened) under the ETF and ITF loading conditions. Analytical expressions were
 522 derived based on the yield-line models, and Equations (18) and (21) were developed [39, 40]
 523 to determine the yield capacity of fastened lipped channel sections under the ETF and ITF
 524 loading conditions, respectively.

525 For the ETF loading condition,

$$526 \quad P_y = f_y N_m \left(-2r_m + \sqrt{4r_m^2 + t^2 \frac{N^*}{N_m}} \right) \quad (18)$$

$$527 \quad N^* = 2N_m + \frac{4}{\sqrt{3}}(h + 2r_m) \quad (19)$$

$$528 \quad N_m = N + 2.5r_{ext} + (h/2) \quad (20)$$

529 For the ITF loading condition,

$$530 \quad P_y = \frac{1}{2} f_y N_m (\sqrt{16r_m^2 + 6t^2} - 4r_m) \quad (21)$$

$$531 \quad N_m = \min (L; N + 5r_{ext} + 3h) \quad (22)$$

532 where N_m is the length of yield line (mm), N^* is an auxiliary parameter (length in yield-line
 533 method) (mm), r_{ext} is the external bent radius (mm) and r_m is the midline bent radius (mm).

534 These formulae are employed in this study to calculate the yield load of fastened ALC sections
 535 under both loading conditions. Figure 15 display the typical plastic failure mechanism proposed
 536 by Natário et al. [39, 40] as well as von-Mises stress distributions observed at the ultimate
 537 failure stage for the ETF and ITF loading conditions.

538 6.3 Proposed Direct Strength method (DSM)-based approach

539 In this research, a DSM-based approach is developed based on the elastic buckling load (P_{cr})
 540 (Section 6.1), the yield load (P_y) (Section 6.2), and the experimental as well as numerical data
 541 for fastened ALC sections under the ETF and ITF loading conditions. Using a non-linear
 542 regression procedure, the DSM-based formulae (Equations (23) and (24)) were calibrated to
 543 estimate the web crippling strength (P_n) of fastened ALC sections under both loading
 544 conditions.

545 For the ETF loading condition:

$$546 \quad P_n = \begin{cases} P_y & \text{for } \lambda \leq 0.2 \\ 0.3P_y \left[1 - 0.07 \left(\frac{P_{cr}}{P_y} \right)^{0.52} \right] \left(\frac{P_{cr}}{P_y} \right)^{0.52} & \text{for } \lambda > 0.2 \end{cases} \quad (23)$$

547 For the ITF loading condition:

$$548 \quad P_n = \begin{cases} P_y & \text{for } \lambda \leq 0.34 \\ 0.55P_y \left[1 - 0.138 \left(\frac{P_{cr}}{P_y} \right)^{0.58} \right] \left(\frac{P_{cr}}{P_y} \right)^{0.58} & \text{for } \lambda > 0.34 \end{cases} \quad (24)$$

549 where λ is the web crippling slenderness ($\lambda = \sqrt{P_y/P_{cr}}$).

550 Figures 16 (a) and (b) compare the load ratio P_n/P_y against the web crippling slenderness (λ).
 551 A clear trend signifying the relationship between P_n/P_y and λ can be seen for both the ETF and
 552 ITF loading conditions. This generally indicates the reliability of the proposed elastic buckling
 553 coefficient (Equation (17)), and the suitability of the yield-line theory developed by Natário et
 554 al. [39,40] for determining the yield load (P_y) for cold-formed steel members to be applied to
 555 aluminium members. Further, having no data points closer to the plastic plateau ($P_n/P_y=1$)
 556 implies that the ALC sections are primarily governed by buckling failure and a combination of
 557 buckling and plastic failure due to the low value of elastic modulus. Table 6 gives the mean

558 values of the ultimate-to-DSM predicted capacity ratios as 1.01 and 1.01, while the
 559 corresponding COV values are 0.11 and 0.13 for the ETF and ITF loading conditions,
 560 respectively.

561 7 Reliability analysis

562 The statistical model recommended by the North American Specification [41] are generally
 563 used to calculate the capacity resistance factor (ϕ_w). The variation of material, fabrication and
 564 loading effects is considered in this model (Equation (25)).

$$565 \quad \phi_w = 1.5M_m F_m P_m e^{-\beta_0 \sqrt{V_M^2 + V_F^2 + C_n V_P^2 + V_Q^2}} \quad (25)$$

566 where P_m and V_p are the mean value and the COV of the test-to-predicted load ratio,
 567 respectively, F_m and $V_F = 1.0, 0.05$ are the mean value and COV of the fabrication factor,
 568 respectively, $M_m, V_M = 1.1, 0.06$ are the mean value and COV of the material factor,
 569 respectively, $V_Q = 0.21$ is the COV of the load effect, $C_n = n^2 - 1/n^2 - 3n$ is the correction
 570 factor depending on the number of tests n and β_0 is the target reliability index for beams ($\beta_0 \geq$
 571 2.5).

572

573 Table 6 gives the respective resistance factor (ϕ_w) and reliability indexes (β_0) for the
 574 predictions of the international design rules, modified equations and proposed DSM formulae.
 575 The results showed that the reliability indexes (β_0) calculated based on the recommended
 576 resistance factors (ϕ_w) given in the international specifications are less than the target value
 577 ($\beta_0 < 2.5$) which indicates their unreliability. However, the reliability indexes (β_0) for the
 578 modified and proposed DSM equations and based on our recommended resistance factors (ϕ_w)
 579 are equal or exceed the target value ($\beta_0 \geq 2.5$). Hence, it is suggested to use $\phi_w = 0.90$ for all
 580 modified equations, except Equation 12, and $\phi_w = 0.85$ for the proposed DSM-based approach
 581 as well as Equation (12).

582 8 Conclusions

583 This paper describes a numerical study of fastened roll-formed ALC sections under web
 584 crippling action with two-flange loading conditions. 38 numerical models were firstly
 585 developed and validated with the results of the experimental study conducted by the authors in
 586 the past. A comprehensive parametric study was then conducted to further study the influence
 587 of various parameters including sectional geometries, bearing lengths and aluminium alloy
 588 grades on the web crippling capacities. The acquired large database containing numerical and

589 previous experimental results was then used to explore the effect of restrained flanges on the
590 web crippling capacity of the ALC sections. The web crippling capacities of these sections
591 have increased due to flange restraining up to 88% and 45% under the ETF and ITF loading
592 conditions, respectively. Both the accuracy and reliability of the current design rules
593 recommended by the international specifications as well as the modified equations with the
594 association of the proposed fastening factor were evaluated. It was found that the design rules
595 specified in the current international guidelines are unsafe with a large coefficient of variation
596 to estimate the web crippling capacities, apart of AS/NZS 1664.1 for the ITF loading condition.
597 On the other hand, the modified equations can accurately predict the web crippling capacity of
598 fastened ALC sections. The development of DSM-design approach for fastened roll-formed
599 aluminium sections is also presented in this study. The elastic buckling analyses were carried
600 out, and a predictive approach was proposed to estimate the buckling load. Further, the existing
601 analytical expressions derived based on the Yield-Line Theory to determine the plastic load for
602 cold-formed steel members were found to be suitable and applicable for fastened ALC sections.
603 The outcomes of this study can be considered for potential inclusion in the relevant
604 international specifications to improve the accuracy and reliability of the design rules.

605 **Acknowledgements**

606 The authors are grateful to Griffith University for providing the necessary technical support
607 and test facilities to conduct this project, and to Mr Robert Price from BlueScope Building
608 Components Pty Ltd for supplying the test specimens.

609 **References**

- 610 [1] Mazzolani FM. Structural applications of aluminium in civil engineering. *Struct Eng*
611 *Intern* 2006;16(4):280-5.
- 612 [2] American Iron and Steel Institute. Standard test method for determining the web
613 crippling strength of cold-formed steel beams. AISI S909, Washington DC, USA; 2008.
- 614 [3] Bock M, Theofanous M, Dirar S, Raybone P. Assessment of web crippling design
615 provisions for application to proprietary soldier beams. *Struct* 2019;20:147-56.
- 616 [4] Gunalan S, Mahendran M. Web crippling tests of cold-formed steel channels under two
617 flange load cases. *J Const Steel Res* 2015;110:1-15.
- 618 [5] Gunalan S, and Mahendran M. .Experimental study of unlipped channel beams subject
619 to web crippling under one flange load cases. *Adv Steel Constr* 2019;15(2):165-72.

- 620 [6] Sundararajah L, Mahendran M, Keerthan P. New design rules for lipped channel beams
621 subject to web crippling under two-flange load cases. *Thin-Walled Struct*
622 2017;119:421-37.
- 623 [7] Sundararajah L, Mahendran M, Keerthan P. Experimental studies of lipped channel
624 beams subject to web crippling under two-flange load cases. *J Struct Eng* 2016;142(9):
625 :04016058.
- 626 [8] Sundararajah L, Mahendran M, Keerthan P. Web crippling studies of SupaCee sections
627 under two flange load cases. *Eng Struct* 2017;153:582-97.
- 628 [9] Keerthan P, Mahendran M, Steau E. Experimental study of web crippling behaviour of
629 hollow flange channel beams under two flange load cases. *Thin-Walled Struct*
630 2014;85:207-19.
- 631 [10] Uzzaman A, Lim JBP, Nash D, Rhodes J, and Young B. Cold-formed steel sections
632 with web openings subjected to web crippling under two-flange loading conditions—
633 Part I: Tests and finite element analysis. *Thin-Walled Struct* 2012;56:38–48.
- 634 [11] Uzzaman A, Lim JBP, Nash D, Rhodes J, and Young B. Web crippling behaviour of
635 cold-formed steel channel sections with offset web holes subjected to interior-two-
636 flange loading. *Thin-Walled Struct* 2012;50(1):76–86.
- 637 [12] Steau E, Mahendran M, Keerthan P. Web crippling tests of rivet fastened rectangular
638 hollow flange channel beams under two flange load cases. *Thin-Walled Struct*
639 2015;95:262-275.
- 640 [13] Steau E, Keerthan P, Mahendran M. Web crippling capacities of rivet fastened
641 rectangular hollow flange channel beams under one flange load cases. *Steel Constr*
642 2016;9(3):222-239.
- 643 [14] Bhakta BH, LaBoube RA, Yu WW. The effect of flange restraint on web crippling
644 strength. Final report, University of Missouri-Rolla, Rolla, MO, USA; 1992.
- 645 [15] Gerges RR, and Schuster RM. Web crippling of single web cold formed steel members
646 subjected to end one-flange loading. Proceedings of the 14th International specialty
647 conference on cold-formed steel structures; 1998 October. 1998. Missouri, U.S.A.
- 648 [16] Macdonald M, Don MH, Kotełko M, Rhodes J. Web crippling behaviour of thin-
649 walled lipped channel beams. *Thin-Walled Struct* 2011;49(5):682-90.

- 650 [17] Janarthanan B, Mahendran M, and Gunalan S. Bearing capacity of cold-formed
651 unlippped channels with restrained flanges under EOF and IOF load cases. *Steel*
652 *Constr* 2015;8(3):146-154.
- 653 [18] Janarthanan B, Mahendran M, and Gunalan S. Numerical modelling of web crippling
654 failures in cold-formed steel unlippped channel sections. *J. Constr Steel Res*
655 2019;158:486-501.
- 656 [19] Janarthanan B, Sundararajah L, Mahendran M, Keerthan P, and Gunalan S. Web
657 crippling behaviour and design of cold-formed steel sections. *Thin-Walled Struct*
658 2019;140:387-403.
- 659 [20] Beshara B, and Schuster R M. Web crippling of cold formed steel C- and Z- sections. .
660 *Proceedings of the 15th International specialty conference on cold-formed steel*
661 *structures, Department of Civil Engineering Center for Cold- Formed Steel Structures;*
662 2000. Rolla, MO.
- 663 [21] Wang YQ, Wang ZX, Yin FX, Yang L, Shi YJ, Yin J. Experimental study and finite
664 element analysis on the local buckling behavior of aluminium alloy beams under
665 concentrated loads. *Thin-Walled Struct* 2016;105:44-56.
- 666 [22] Zhou F. and Young B. “Aluminium alloy channels subjected to web crippling.” *Adv*
667 *in Struct Eng* 2019; 22(7), 1617-1630.
- 668 [23] Zhou F, Young B. Aluminum tubular sections subjected to web crippling—Part I. *Thin-*
669 *Walled Struct* 2008;46(4):339-51.
- 670 [24] Young B, Zhou F. Aluminium tubular sections subjected to web crippling—Part II:
671 Proposed design equations. *Thin-Walled Struct* 2008;46(4):352-361.
- 672 [25] Zhou F, Young B, Zhao X.L. Tests and design of aluminium tubular sections subjected
673 to concentrated bearing load. *J Struct Eng* 2009;135(7):816-817.
- 674 [26] Chen Y, Chen X, Wang C. Aluminum tubular sections subjected to web crippling. *Thin-*
675 *Walled Struct* 2015;90:49-60.
- 676 [27] Su MN, Young B. Design of aluminium alloy stocky hollow sections subjected to
677 concentrated transverse loads. *Thin-Walled Struct* 2018;124:546-57.
- 678 [28] Alsanat H, Gunalan S, Guan H, Keerthan P, Bull J. Experimental study of aluminium
679 lippped channel sections subjected to web crippling under two flange load cases. *Thin-*
680 *Walled Struct* 2019;141:460-476.

- 681 [29] Alsanat H, Gunalan S, Guan H, Keerthan P, K. & Tsavdaridis K. D. Web crippling
682 behaviour and design for aluminium lipped channel sections under two flange loading
683 conditions. *Thin-Walled Struct* 2019; 144:106265.
- 684 [30] Alsanat H, Gunalan S, Poologanathan K, Guan H, Baniotopoulos C. Web Crippling for
685 fastened aluminium lipped channel sections under two flange loading conditions. *J*
686 *Struct Eng* 2019. (in press)
- 687 [31] Standards Australia/Standards New Zealand. Australia/New Zealand Standard AS/NZS
688 1664.1 Aluminium structures - Part 1: Limit state design. Sydney, Australia; 1997.
- 689 [32] Standards Australia/Standards New Zealand. Australia/New Zealand Standard AS/NZS
690 4600 Cold-formed steel structures. Sydney, Australia; 2018.
- 691 [33] EN 1993-1-3. Eurocode 3: Design of steel structures – part 1-3: general rules –
692 supplementary rules for cold-formed members and sheeting. European Committee for
693 Standardization, Brussels; 2006.
- 694 [34] Simulia. ABAQUS Standard User’s Manual, Version 6.14, Rhode Island, USA; 2013.
- 695 [35] Natário P, Silvestre N, Camotim D. Web crippling failure using quasi-static FE models.
696 *Thin-Walled Struct* 2014;84:34-49.
- 697 [36] Su MN, Young B. Design of aluminium alloy stocky hollow sections subjected to
698 concentrated transverse loads. *Thin-Walled Struct* 2018;124:546-57.
- 699 [37] EN 1999-1-4. Eurocode 9: Design of aluminium structures - Part 1.4: Cold-formed
700 structural sheeting. European Committee for Standardization, Brussels; 2007.
- 701 [38] Schafer BW. The direct strength method of cold-formed steel member design. *J Constr*
702 *Steel Res* 2008;64(7-8):766-78.
- 703 [39] Natário P, Silvestre N, Camotim D. Direct strength prediction of web crippling failure
704 of beams under ETF loading. *Thin-Walled Struct* 2016;98:360-74.
- 705 [40] Natário P, Silvestre N, Camotim D. Web crippling of beams under ITF loading: A novel
706 DSM-based design approach. *J Const Steel Res* 2017;128:812-24.
- 707 [41] American Iron and Steel Institute (AISI). Specifications for the cold-formed steel
708 structural members, cold-formed steel design manual. AISI S100, Washington DC,
709 USA; 2012.

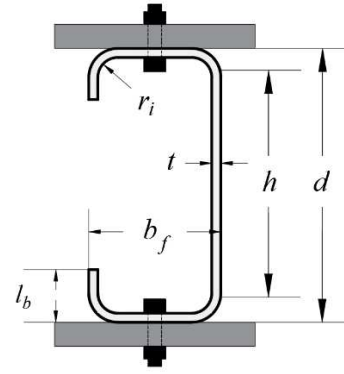
710



(a) ETF test



(b) ITF test



(c) Cross section profile

711

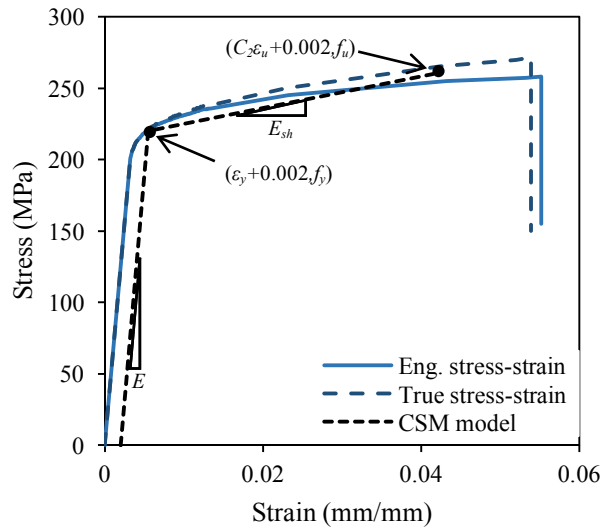
712

713

714

715

Figure 1: Fastened web crippling test set-up and ACL section profile [30]



716

717

Figure 2: Typically measured stress-strain curve and bi-linear CSM model [36] for 5052-H36 aluminium alloy

718

719

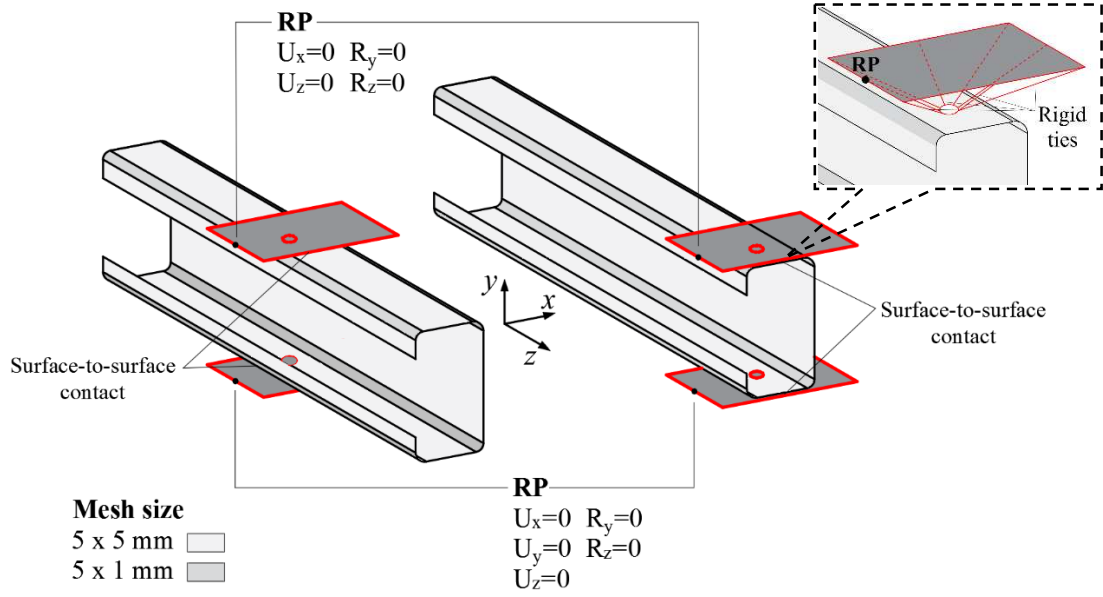
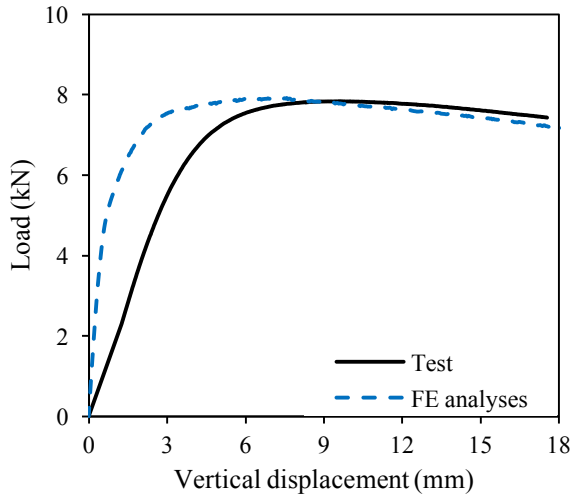
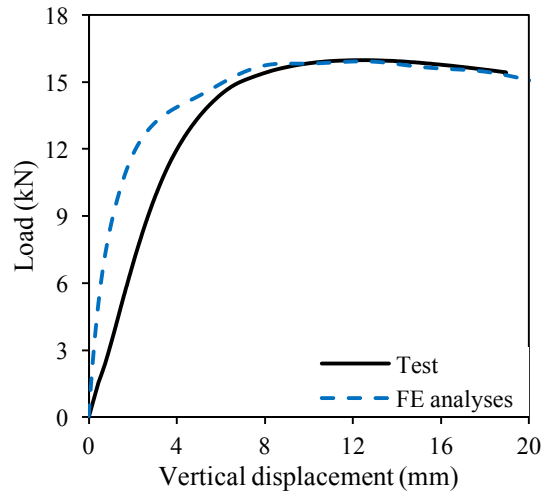


Figure 3: Overview of the assigned boundary conditions and mesh size distributions in the web crippling models (RP: Reference Point)

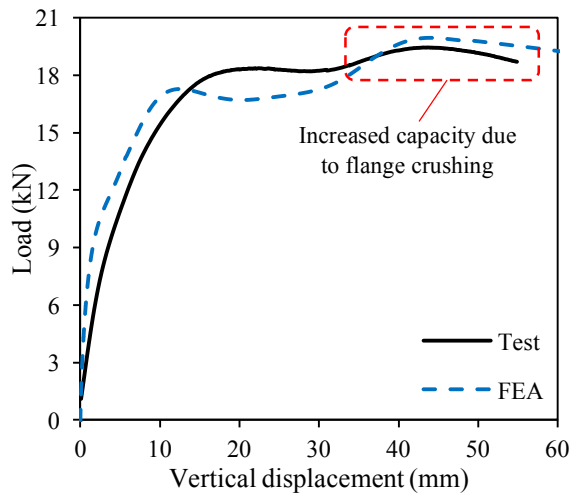
720
 721
 722
 723
 724
 725
 726
 727
 728
 729
 730
 731
 732
 733
 734
 735
 736
 737
 738
 739
 740
 741
 742
 743
 744
 745
 746
 747
 748



(a) ETF-15030-N50



(b) ITF-25025-N100



(c) ITF-20030-N25

Figure 4: Comparison of experimental and numerical load versus vertical displacement curves

749
750

751
752
753
754
755

756

757

758

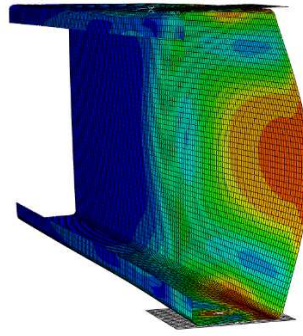
759

760

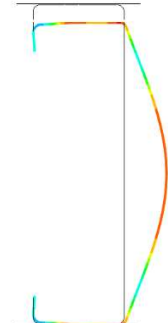
761



Test specimen



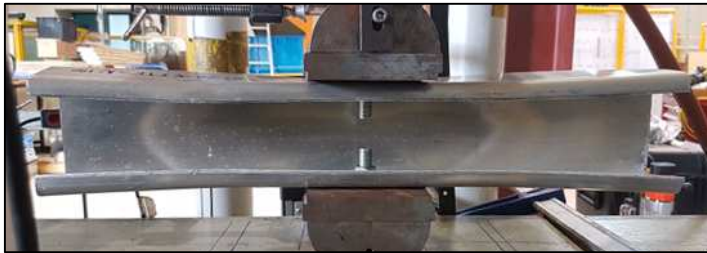
FE model



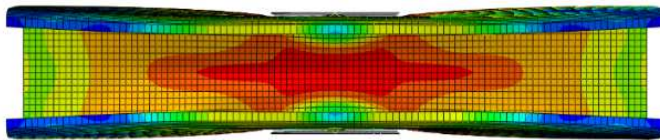
FE cross section

(a) ETF-25025-N100 (web crippling)

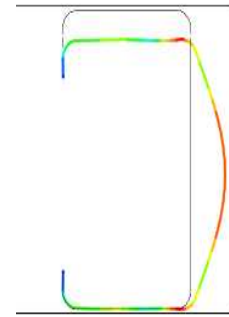
762
763
764
765
766



Test specimen



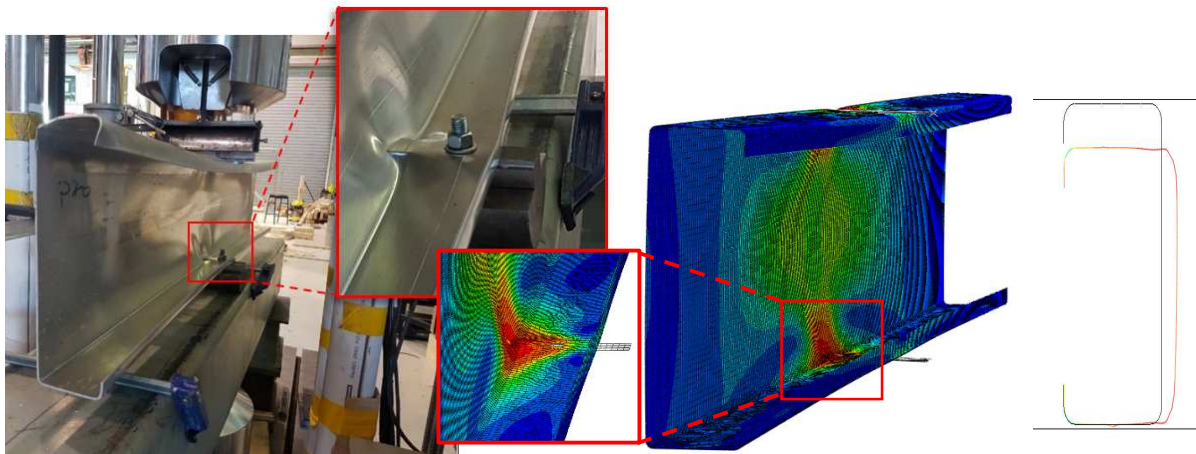
FE model



FE cross section

(b) ITF-10030-N100 (web crippling)

767
768



Test specimen

FE model

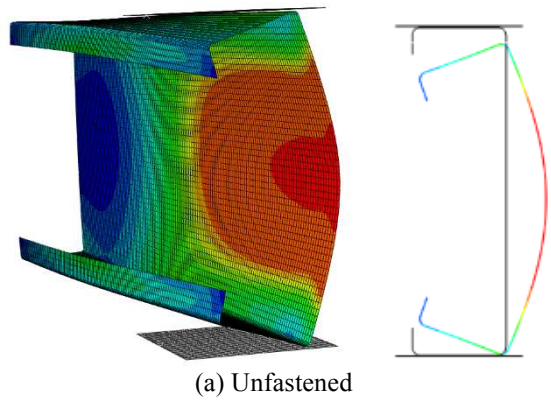
FE cross section

(c) ITF-25025-N25 (flange crushing)

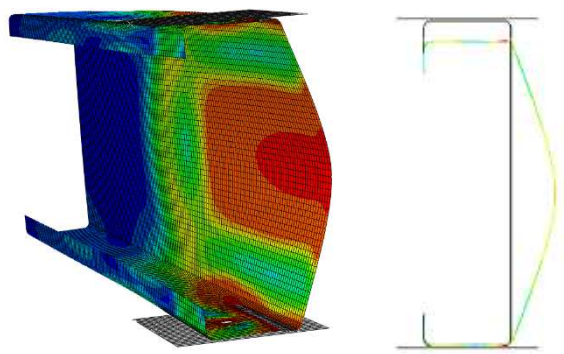
Figure 5: Comparison of experimental and numerical failure modes

769
770
771
772
773

774
775
776



(a) Unfastened



(b) Fastened

Figure 6: Web crippling failure modes for unfastened and fastened specimens

777
778
779
780
781

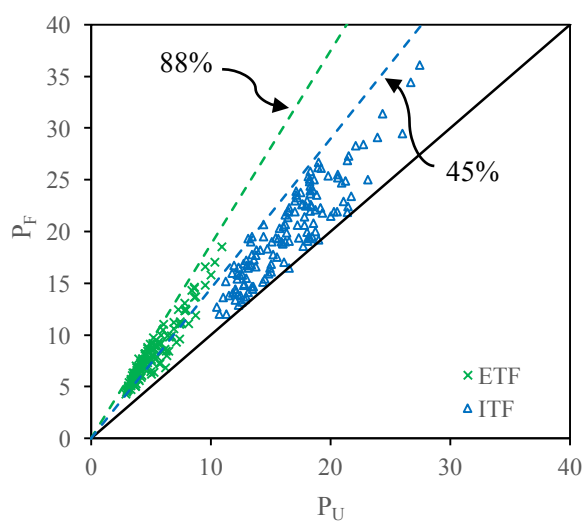
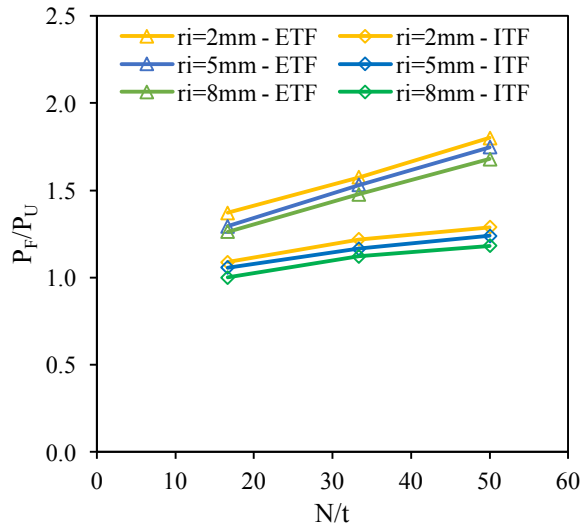


Figure 7: Comparison between the web crippling failure capacities of fastened (P_F) and unfastened (P_U) models

782
783
784
785
786
787



788

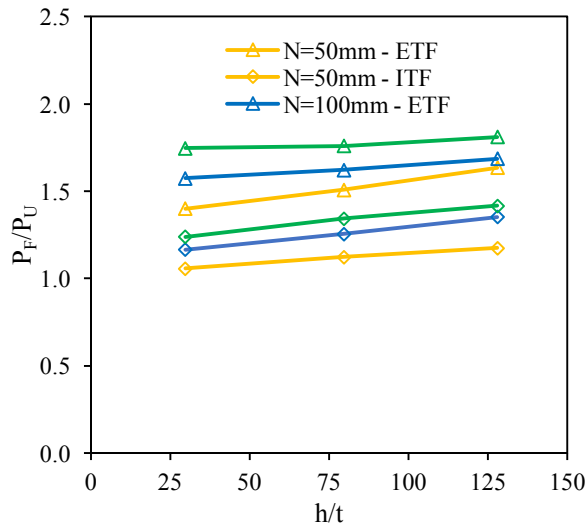
789

790

791

792

Figure 8: Web crippling capacity ratio (P_F/P_U) versus bearing length ratio (N/t) with different inside bent radii (models with $h/t = 32$ and $f_y = 179$ MPa)



793

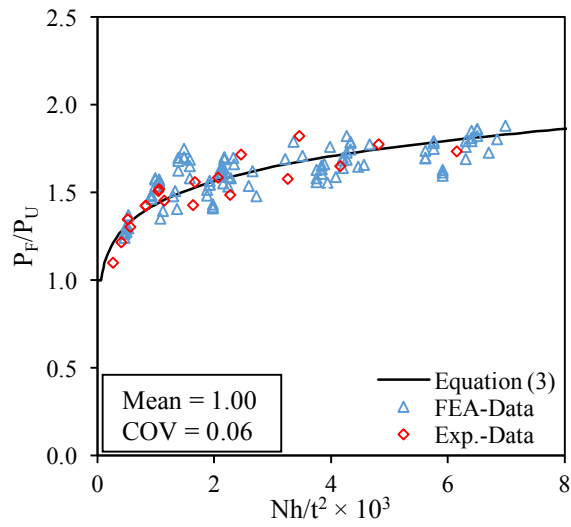
794

795

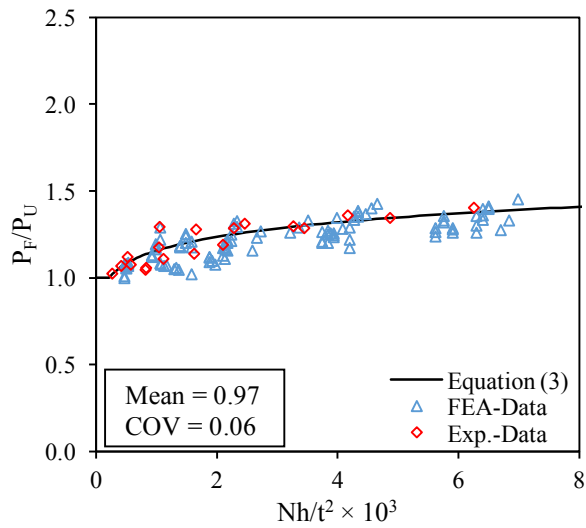
796

797

Figure 9: Web crippling capacity (P_F/P_U) versus web slenderness ratio (h/t) with different bearing lengths (models with $r_i = 5$ mm and $f_y = 179$ MPa)



(a) ETF loading condition

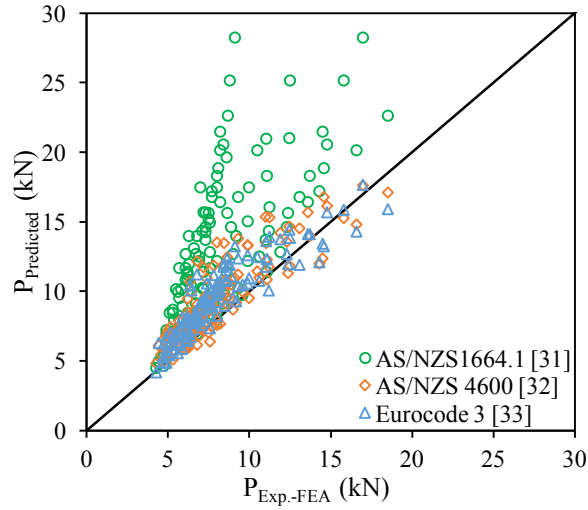


(b) ITF loading condition

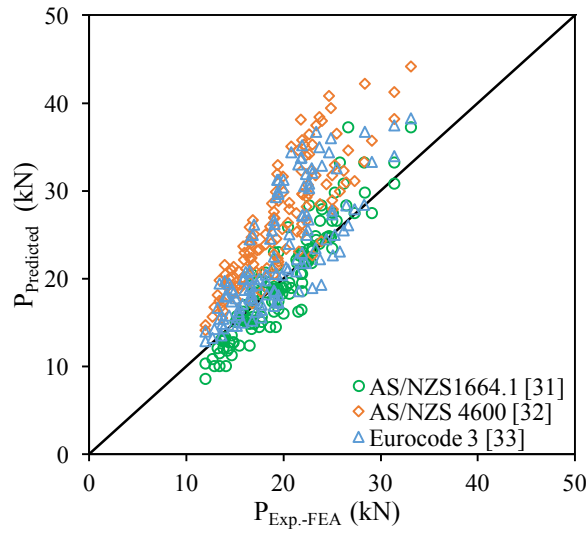
Figure 10: Influence of fastened-to-unfastened capacity (P_F/P_U) against the geometrical factor Nh/t^2

798
799

800
801
802
803
804
805
806



(a) ETF loading condition

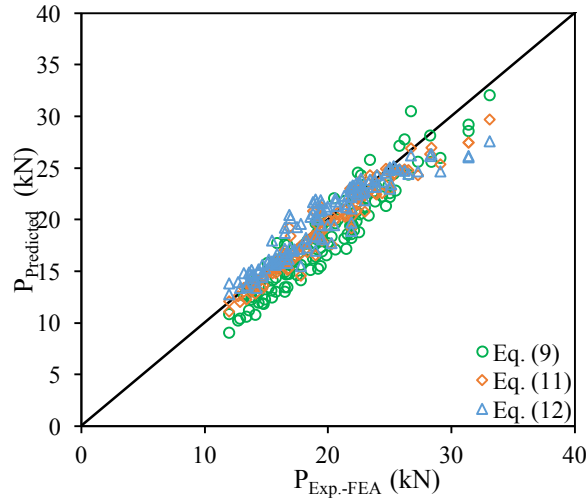


(b) ITF loading condition

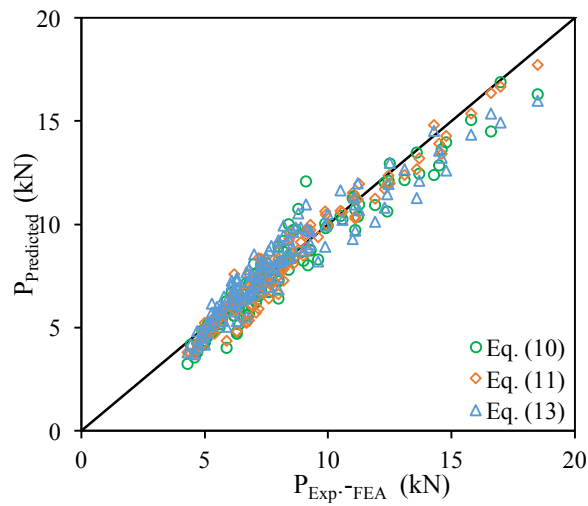
Figure 11: Comparison between experimental and numerical web crippling capacities and predictions of current international specifications

807
808
809

810
811
812
813
814
815
816
817
818
819



(a) ETF loading condition



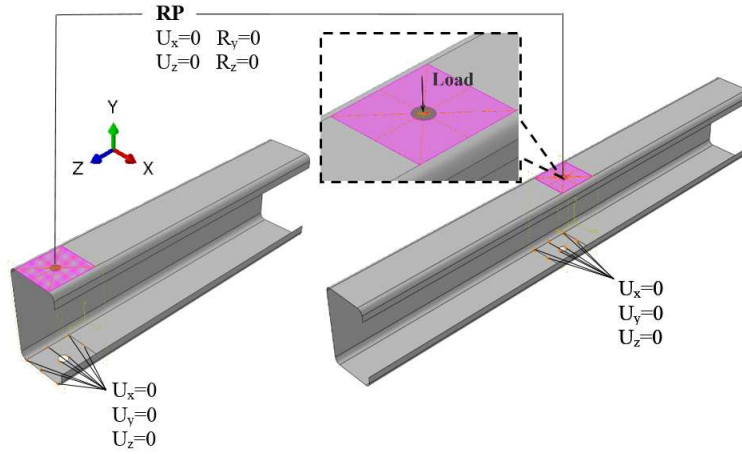
(b) ITF loading condition

Figure 12: Comparison between experimental and numerical web crippling capacities and predictions of modified equations (Equations (9-13))

820
821

822
823
824
825
826
827
828
829
830
831

832



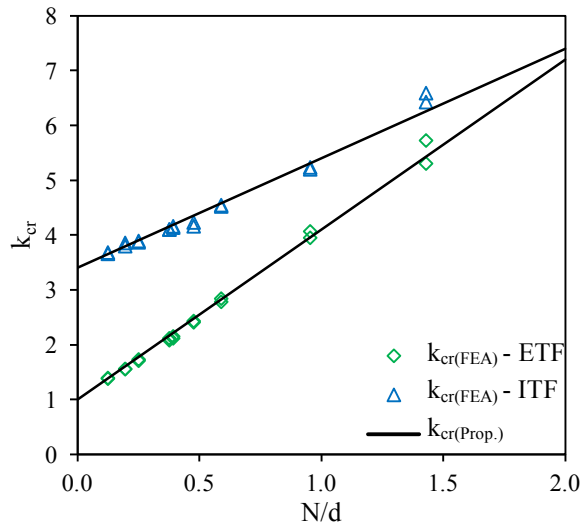
833

834

Figure 13: Assigned boundary conditions in the buckling model for fastened ALC sections

835

836



837

838

Figure 14: Comparison between the proposed elastic buckling coefficients ($k_{cr(Prop.)}$) and FEA elastic buckling coefficients ($k_{cr(FEA)}$) for different N/d ratios

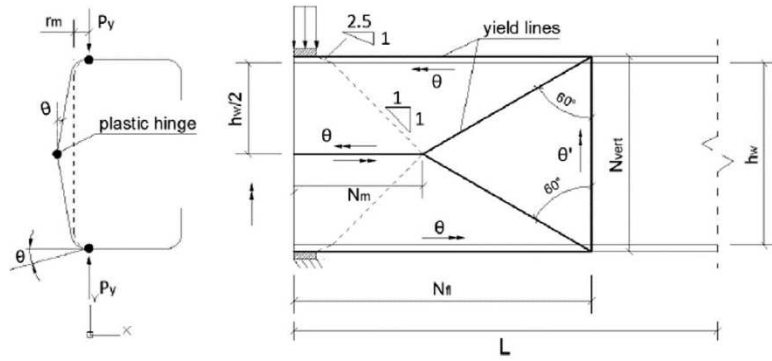
839

840

841

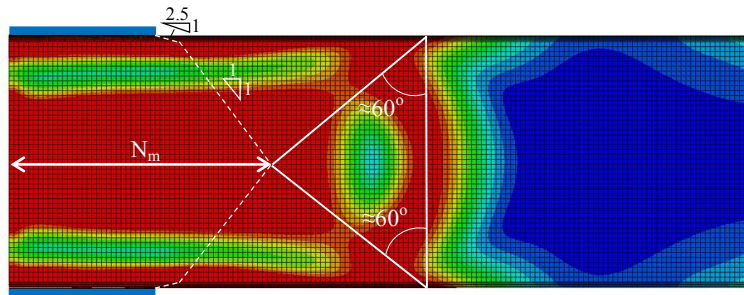
842

843



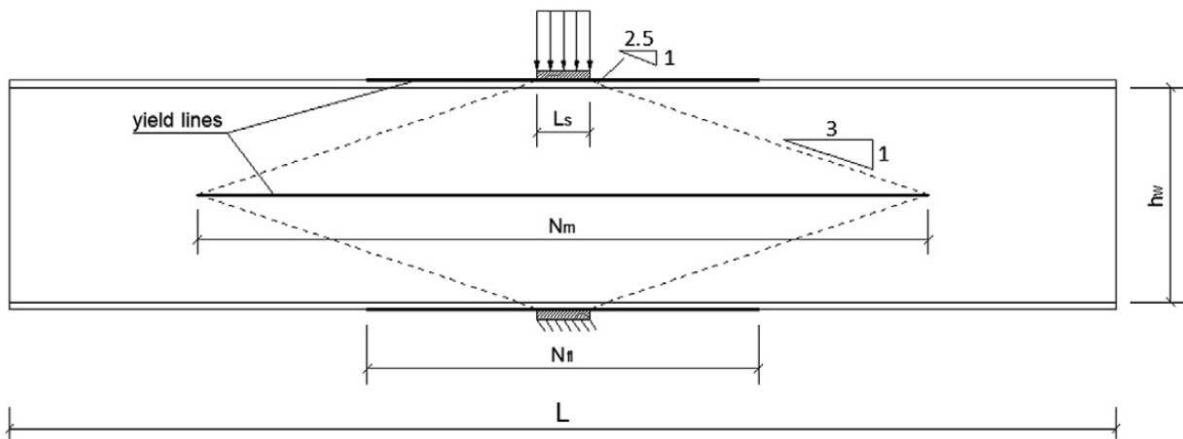
844
845

(a) Plastic mechanism - fastened ETF loading condition [39]



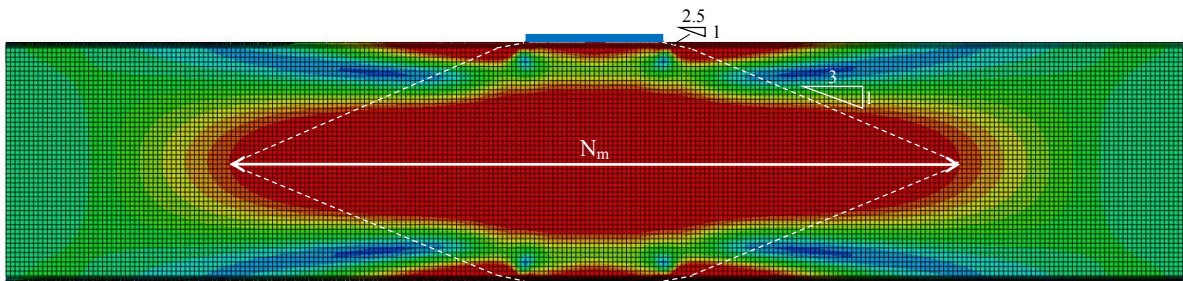
846
847

(b) von-Mises stress distributions - fastened ETF loading condition



848
849

(c) Plastic mechanism - fastened ITF loading condition [40]

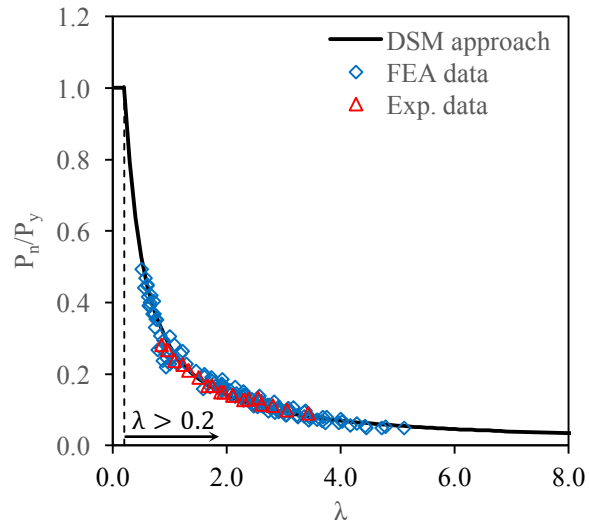


850
851

(d) von-Mises stress distributions - fastened ITF loading condition

852
853
854

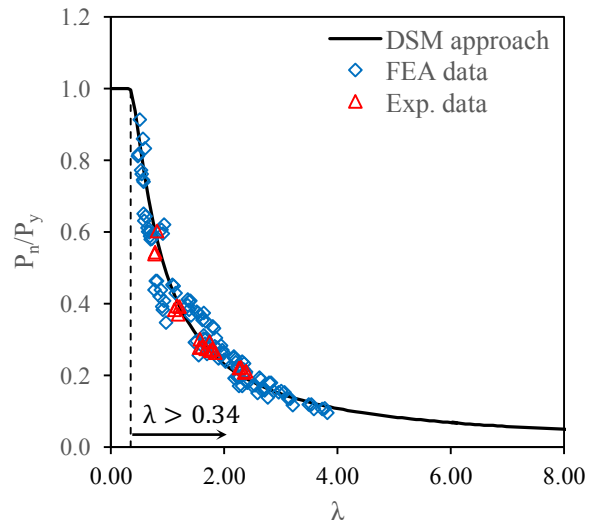
Figure 15: Plastic mechanism proposed by Natário et al. [39, 40] and von-Mises stress distributions at the ultimate load



855

856

(a) ETF loading condition



857

858

(b) ITF loading condition

859 Figure 16: Comparison between the web crippling strength using proposed DSM-based approach and FEA-
860 experimental data

861

862

863

864

865

866

867

868

869

870
871

Table 1: Comparison of experimental and FEA web crippling capacities for ETF loading condition

Specimen	d (mm)	b_f (mm)	l_b (mm)	t (mm)	r_i (mm)	L (mm)	$P_{Exp.}$ (kN)	P_{FEA} (kN)	$P_{Exp.}/P_{FEA}$ (kN)
ETF-10030-N25	107.2	60.5	14.8	2.95	4.9	107.2	6.80	7.13	0.95
ETF-10030-N50	106.4	58.3	16.2	2.95	5.0	106.4	8.44	8.59	0.98
ETF-10030-N100	107.2	59.3	15.1	2.95	4.8	316	11.25	12.68	0.89
ETF-15030-N25	156.8	62.9	23.0	2.93	4.9	466	6.37	7.05	0.90
ETF-15030-N50	157.6	63.2	22.3	2.93	5.0	465	7.84	7.91	0.99
ETF-15030-N100	158.4	63.3	21.8	2.92	5.1	465	9.92	10.03	0.99
ETF-15030-N150	155.4	63.4	23.0	2.92	4.9	467	12.45	13.45	0.93
ETF-20025-N25	208.2	74.5	25.4	2.42	5.1	617	4.74	5.01	0.95
ETF-20025-N50	208.0	74.3	25.3	2.43	4.9	615	5.15	5.52	0.93
ETF-20025-N100	207.2	74.2	25.8	2.43	5.0	615	6.19	6.57	0.94
ETF-20025-N150	204.1	75.9	26.4	2.43	4.8	615	7.51	8.17	0.92
ETF-20030-N25	204.5	74.9	27.5	2.9	4.6	611	6.45	7.07	0.91
ETF-20030-N50	208.3	73.1	27.6	2.9	5.0	615	7.37	7.60	0.97
ETF-20030-N100	204.4	75.5	27.6	2.89	4.6	613	8.64	9.41	0.92
ETF-20030-N150	208.2	73.4	27.2	2.89	5.0	615	11.05	11.31	0.98
ETF-25025-N25	259.9	80.7	23.5	2.43	4.4	765	4.45	4.60	0.97
ETF-25025-N50	259.8	76.2	23.8	2.44	4.9	765	4.90	4.89	1.00
ETF-25025-N100	262.2	76.1	22.6	2.44	4.8	765	6.20	5.76	1.08
ETF-25025-N150	260.4	76.2	23.5	2.45	4.6	765	7.20	6.91	1.04
Mean									0.96
COV									0.05

872

873

874

Table 2: Comparison of experimental and FEA web crippling capacities for ITF loading condition

Specimen	d (mm)	b_f (mm)	l_b (mm)	t (mm)	r_i (mm)	L (mm)	$P_{Exp.}$ (kN)	P_{FEA} (kN)	$P_{Exp.}/P_{FEA}$ (kN)
ITF-10030-N25	106.8	59.3	14.3	2.94	4.8	527	21.88	21.16	1.03
ITF-10030-N50	106.5	59.4	14.8	2.95	4.9	525	20.79	19.46	1.07
ITF-10030-N100	106.2	59.6	14.4	2.94	4.8	523.5	23.68	22.85	1.04
ITF-15030-N25	156.6	62.6	22.6	2.93	4.8	774	19.99	20.40	0.98
ITF-15030-N50	156.8	62.4	22.7	2.92	4.9	775	19.34	19.59	0.99
ITF-15030-N100	156.3	62.1	22.7	2.92	4.8	776	22.99	23.61	0.97
ITF-15030-N150	156.7	62.5	22.8	2.93	4.9	774	23.99	25.98	0.92
ITF-20025-N25	206.3	74.0	26.3	2.43	4.6	1028	13.41	14.21	0.94
ITF-20025-N50	207.3	73.3	26.0	2.44	4.9	1022	13.93	14.00	1.00
ITF-20025-N100	207.4	73.9	26.3	2.43	5.0	1019	15.83	17.28	0.92
ITF-20025-N150	207.5	73.4	26.9	2.44	4.6	1021	16.52	18.70	0.88
ITF-20030-N25	205.5	74.5	31.6	2.9	4.4	1022	19.46	19.55	1.00
ITF-20030-N50	206.7	75.3	27.4	2.93	4.8	102	19.97	19.52	1.02
ITF-20030-N100	206.4	74.4	26.7	2.9	4.8	1021	22.63	23.33	0.97
ITF-20030-N150	206.6	74.5	26.7	2.89	4.6	1022	22.67	24.68	0.92
ITF-25025-N25	259.8	76.1	22.1	2.43	4.4	1273	14.21	13.38	1.06
ITF-25025-N50	260.1	76.0	22.4	2.42	4.5	1274	14.05	13.99	1.00
ITF-25025-N100	259.9	76.3	22.5	2.43	4.5	1269	15.99	15.99	1.00
ITF-25025-N150	259.8	76.2	22.2	2.43	4.5	1275	16.72	16.40	1.02
Mean									0.99
COV									0.05

875 Table 3. Mechanical properties of aluminium sections used in the numerical simulations [30]

Section	E (GPa)	$\sigma_{0.2,Eng}$ (MPa)	$\sigma_{0.2,true}$ (MPa)	$\sigma_{u,Eng.}$ (MPa)	$\sigma_{u,True}$ (MPa)	$\varepsilon_{u,Eng.}$ (%)	$\varepsilon_{u, True}$ (%)
10030	65.05	210	223	259	274.93	6.15	5.97
15030	63.55	206	217	248	261.76	5.55	5.40
20025	63.95	214	225	260	273.13	5.05	4.93
20030	64.13	212	226	257	273.63	6.47	6.27
25025	64.34	216	230	265	282.70	6.68	6.47

876

877 Table 4: Parametric study model details of ALC sections under ETF and ITF loading conditions

Loading condition	Section	N (mm)	h/t	r_i (mm)	Aluminium hardening	Number of models	
ETF	10030	50,100,150	27.7 - 31.7	2, 5, 8	H32, H36, H38	27	
	15025	50,100,150	53.6 - 58.4	2, 5, 8	H36	9	
	25025	50,100,150	96 - 98.4	2, 5, 8	H32, H36, H38	27	
	25030	50,100,150	77.7 - 81.7	2, 5, 8	H36	9	
	30025	50,100,150	110.6 - 116.4	2, 5, 8	H36	9	
	40030	50,100,150	126-130	2, 5, 8	H32, H36, H38	27	
	Experiment						19
	FE-validation						19
	Sub-total						146
	ITF	10030	50,100,150	27.7 - 31.7	2, 5, 8	H32, H36, H38	27
15025		50,100,150	53.6 - 58.4	2, 5, 8	H36	9	
25025		50,100,150	96 - 98.4	2, 5, 8	H32, H36, H38	27	
25030		50,100,150	77.7 - 81.7	2, 5, 8	H36	9	
30025		50,100,150	110.6 - 116.4	2, 5, 8	H36	9	
40030		50,100,150	126-130	2, 5, 8	H32, H36, H38	27	
Experiment						19	
FE-validation						19	
Sub-total						146	
Total						292	

878 Note: H32 : (yield stress (f_y) = 145 MPa, ultimate stress (f_u)= 214 MPa and Young's Modulus (E) = 70 GPa)

879 H36 : (f_y = 179 MPa, f_u = 255 MPa and E = 69.3 GPa)

880 H38 : (f_y = 207 MPa, f_u = 268 MPa and E = 70.3 GPa)

881

882

Table 5: Geometrical coefficients used in Equations (6) and (11)

Design rule	Loading condition	C	C_R	C_N	C_h
AS/NZS 4600 [32]	ETF	7.50	0.08	0.12	0.048
	ITF	20.00	0.10	0.08	0.031
Modified [28]	ETF	0.273	0.21	0.16	0.06
	ITF	0.78	0.17	0.04	0.03

883
884

Table 6: Comparison of mean and COV values for ultimate-to-predicted web crippling capacity ratios ($P_{Exp.-FEA}/P_{Predicted}$)

Rule	Loading condition	Equation	Mean	COV	ϕ_w	β_0
Current	ETF	AS/NZS 1664.1 [31]	0.68	0.26	0.90	0.64
		AS/NZS 4600 [32]	0.55	0.13	0.85	0.25
		Eurocode 3 [33]	0.86	0.13	1.00	1.30
	ITF	AS/NZS 1664.1 [31]	1.04	0.13	0.90	2.48
		AS/NZS 4600 [32]	0.65	0.11	0.85	0.91
		Eurocode 3 [33]	0.87	0.17	1.00	1.29
Modified	ETF	Equation (9)	1.06	0.11	0.90	2.67
		Equation (11)	1.04	0.08	0.90	2.69
		Equation (12)	0.99	0.13	0.85	2.50
	ITF	Equation (10)	1.10	0.09	0.90	2.89
		Equation (11)	1.03	0.06	0.90	2.72
		Equation (13)	1.04	0.10	0.90	2.65
Proposed	ETF	DSM approach	1.01	0.11	0.85	2.70
	ITF	DSM approach	1.01	0.13	0.85	2.58

885
886

Table 7: Comparison of FEA and proposed critical buckling loads – ETF loading condition

Specimen	r_i (mm)	$P_{cr(FEM)}$ (kN)	$k_{cr(FEA)}$	$k_{cr(Prop.)}$	$P_{cr(Prop.)}$ (kN)	$P_{cr(FEM)}/P_{cr(Prop.)}$
ETF-10030-N50	5.00	39.60	2.41	2.43	39.98	0.99
ETF-10030-N50	8.00	39.90	2.42	2.43	39.98	1.00
ETF-10030-N100	5.00	66.80	4.06	3.86	63.49	1.05
ETF-10030-N100	8.00	65.00	3.95	3.86	63.49	1.02
ETF-10030-N150	5.00	94.20	5.72	5.29	87.01	1.08
ETF-10030-N150	8.00	87.30	5.30	5.29	87.01	1.00
ETF-25025-N50	5.00	6.10	1.56	1.59	6.23	0.98
ETF-25025-N50	8.00	6.10	1.56	1.59	6.23	0.98
ETF-25025-N100	5.00	8.44	2.15	2.18	8.54	0.99
ETF-25025-N100	8.00	8.30	2.12	2.18	8.54	0.97
ETF-25025-N150	5.00	11.10	2.83	2.76	10.84	1.02
ETF-25025-N150	8.00	10.90	2.78	2.76	10.84	1.01
ETF-40030-N50	5.00	6.00	1.39	1.38	5.94	1.01
ETF-40030-N50	8.00	5.96	1.38	1.38	5.94	1.00
ETF-40030-N100	5.00	7.47	1.73	1.75	7.56	0.99
ETF-40030-N100	8.00	7.37	1.71	1.75	7.56	0.97
ETF-40030-N150	5.00	9.14	2.12	2.13	9.18	1.00
ETF-40030-N150	8.00	8.99	2.08	2.13	9.18	0.98
Mean						1.00
COV						0.03

887

Table 8: Comparison of FEA and proposed critical buckling loads – ITF loading condition

Specimen	r_i (mm)	$P_{cr(FEM)}$ (kN)	$k_{cr(FEA)}$	$k_{cr(Prop.)}$	$P_{cr(Prop.)}$ (kN)	$P_{cr(FEM)}/P_{cr(Prop.)}$
ITF-10030-N50	5.00	68.40	4.16	4.35	71.64	0.95
ITF-10030-N50	8.00	69.60	4.23	4.35	71.64	0.97

ITF-10030-N100	5.00	86.10	5.23	5.30	87.32	0.99
ITF-10030-N100	8.00	85.50	5.19	5.30	87.32	0.98
ITF-10030-N150	5.00	108.30	6.58	6.26	103.00	1.05
ITF-10030-N150	8.00	105.60	6.42	6.26	103.00	1.03
ITF-25025-N50	5.00	14.90	3.80	3.79	14.87	1.00
ITF-25025-N50	8.00	15.10	3.85	3.79	14.87	1.02
ITF-25025-N100	5.00	16.20	4.13	4.18	16.41	0.99
ITF-25025-N100	8.00	16.30	4.16	4.18	16.41	0.99
ITF-25025-N150	5.00	17.70	4.51	4.58	17.95	0.99
ITF-25025-N150	8.00	17.80	4.54	4.58	17.95	0.99
ITF-40030-N50	5.00	15.80	3.66	3.65	15.77	1.00
ITF-40030-N50	8.00	15.90	3.68	3.65	15.77	1.01
ITF-40030-N100	5.00	16.70	3.86	3.90	16.85	0.99
ITF-40030-N100	8.00	16.78	3.88	3.90	16.85	1.00
ITF-40030-N150	5.00	17.70	4.10	4.15	17.93	0.99
ITF-40030-N150	8.00	17.70	4.10	4.15	17.93	0.99
Mean						1.00
COV						0.02

888